Four-dimensional computed tomography analysis of bicuspid aortic valves

Amine Fikani, MD,[a,b] Damian Craiem, PhD,[c] Cyrille Boulogne, PhD,[d] Gilles Soulat, PhD,[e] Elie Mousseaux, PhD,[e] and Jerome Jouan, PhD[f]

ABSTRACT

Objectives: To evaluate the role of 4-dimensional (4D; 3-dimensional [3D] + time) analysis using multiphase cardiac computed tomography (MCCT) in the description of the aortic annulus (AA) of bicuspid aortic valves (BAV) with regard to the latest expert consensus classification.

Methods: Electrocardiography-gated MCCT of 15 patients with BAV were analyzed using in-house software and compared to 15 patients with normal tricuspid aortic valve (TAV). The AA border was pinpointed on 9 reconstructed planes, and the 3D coordinates of the 18 consecutive points were interpolated in 3D using a cubic spline to calculate 3D areas, perimeters, diameters, eccentricity indexes, and global height. Measurements were repeated throughout the cardiac cycle (10 phases). Three additional planes were generated at the level of the left ventricular outflow tract (LVOT), the sinus of Valsalva, and the sinotubular junction.

Results: The annulus area was significantly larger in BAV compared to TAV (mean indexed 3D area, 5.64 ± 0.84 cm^2/m^2 vs 4.3 ± 0.38 cm^2/m^2, respectively; $P < .001$). The AA was also larger in BAV in terms of perimeter, diameters, and height ($P < .001$). The Valsalva sinuses and sinotubular junction also were significantly larger in BAV compared to TAV (mean area in end-diastole, 6.06 ± 1.00 cm^2 vs 4.69 ± 1.00 cm^2 [$P < .001$] and 5.13 ± 1.62 cm^2 vs 3.62 ± 0.99 cm^2 [$P < .001$], respectively). In BAV, 3D AA shape analysis helps distinguish the 3 types of BAV: the 2-sinus type (symmetrical), the fused type, and the partial-fusion type or "form fruste" (both asymmetrical). It also allows determination of the position and height of the nonfunctional commissure. In symmetrical BAV, the nonfunctional commissure was significantly lower than the other commissures (6.01 ± 4.27 mm vs 18.24 ± 3.20 mm vs 17.15 ± 3.60 mm; $P < .001$), whereas in asymmetrical BAV, the 3 commissures were of comparable height (16.38 ± 0.86 mm vs 15.88 ± 1.69 mm vs 15.37 ± 0.88 mm; $P = .316$). There was no difference in AA eccentricity indices between TAV and BAV in all phases of the cardiac cycle; however, there was a spectrum of ellipticity for the other components of the aortic root among the different types of valves: going from TAV to asymmetrical BAV to symmetrical BAV, at end-diastole, the LVOT became more circular and the sinuses of Valsalva became more elliptical.

Conclusions: 3D morphometric analysis of the BAV using MCCT allows identification of the type of BAV and the position and height of the nonfunctional commissure. There are significant differences in the morphology of the aortic root between TAV and the different types of BAV. Further studies are needed to evaluate the impact of 3D analysis on the procedural planning for pathologic BAV. (JTCVS Techniques 2024;27:60-7)

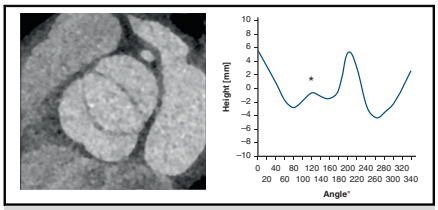

Annulus representation of a bicuspid aortic valve. *Nonfunctional commissure.

CENTRAL MESSAGE

Three-dimensional morphometric analysis of the bicuspid aortic valve using multiphase cardiac computed tomography allows identification of the type of bicuspid aortic valve and the position and height of the nonfunctional commissure.

PERSPECTIVE

In this article, we provide a novel analysis technique of the bicuspid aortic valve based on 4-dimensional computed tomography and specific software developments. There are significant differences in the morphology of the aortic root between tricuspid valves and subtypes of bicuspid valves. These differences can impact procedural preparations in transcatheter aortic valve replacement and in aortic repair.

From the [a]Department of Cardiothoracic and Vascular Surgery, University Medical Center Hôtel-Dieu de France Hospital, Faculty of Medicine, Saint-Joseph University of Beirut, Beirut, Lebanon; [b]XLIM UMR CNRS 7252, Limoges, France; [c]Instituto de Medicina Traslacional, Trasplante y Bioingeniería (IMeTTyB), Universidad Favaloro-CONICET, Buenos Aires, Argentina; [d]Department of Cardiology, Limoges University Hospital, Limoges, France; [e]Department of Cardiovascular Imaging, Assistance Publique Hôpitaux de Paris, Georges Pompidou European Hospital, and Université Paris Cité, Paris-Cardiovascular Research Center, INSERM 970, Paris, France; and [f]Department of Cardiothoracic Surgery, Limoges University Hospital, Limoges, France.

This work was funded by ADETEC and Fédération Française de Cardiologie.

Read at The American Association for Thoracic Surgery Aortic Symposium 2024, New York, New York, April 25-26, 2024.

Received for publication April 19, 2024; revisions received June 4, 2024; accepted for publication June 17, 2024; available ahead of print July 1, 2024.

Address for reprints: Amine Fikani, MD, Faculty of Medicine, Department of Cardiothoracic and Vascular Surgery, University Medical Center Hôtel-Dieu de France Hospital, Saint-Joseph University of Beirut, Boulevard Alfred Naccache - Achrafieh, Beirut, Lebanon (E-mail: aminefikani@gmail.com).

2666-2507

https://doi.org/10.1016/j.xjtc.2024.06.012

Abbreviations and Acronyms

2D = two-dimensional
3D = three-dimensional
4D = four-dimensional
AA = aortic annulus
BAV = bicuspid aortic valve
CO = commissural orientation
CT = computed tomography
ECG = electrocardiography
ED = end-diastole
LVOT = left ventricular outflow tract
MCCT = multiphase cardiac computed tomography annulus
TAV = tricuspid aortic valve
TAVR = transcatheter aortic valve replacement

Bicuspid aortic valve (BAV), the most common congenital heart disease, is characterized by significant heterogeneity in its valvular and aortic phenotypic expressions, as well as in its associated disorders and prognosis.[1-3] Consequently, several classifications have been proposed based on the echocardiographic, surgical, or pathologic appearance of the valve.[4-6] To provide a common language among all disciplines, the International Consensus Classification and Nomenclature for the congenital bicuspid aortic valve condition described 3 types of bicuspid valves: fused type (3 aortic sinuses and 2 cusps of different sizes), 2-sinus type (2 aortic sinuses and 2 symmetrical cusps), and partial-fusion type (3 aortic sinuses and 3 symmetrical cusps).[7] de Kerchove and colleagues[8] proposed a similar repair-oriented classification in which BAV are divided according to their commissural orientation (CO) of the nonfused cusp: type A, symmetrical BAV (CO 160°-180°); type B, asymmetrical BAV (CO 140°-160°); and type C, very asymmetrical BAV (tricuspid-like BAV; CO 120°-140°).

BAV pathologies present several challenges in valve repair surgeries and transcatheter aortic valve replacement (TAVR) planning. In particular, the partially fused very asymmetrical type (tricommissural BAV) can be challenging to repair. Therefore, a careful assessment of the BAV morphology is mandatory. In this context, electrocardiography (ECG)-gated computed tomography (CT) has emerged as a powerful tool to detect BAV with an excellent sensitivity and specificity[9] and also to assess associated aortopathy or to evaluate coronary artery disease.

We previously reported our results on the morphologic temporal analysis of the normal TAV using ECG-gated CT.[10] Using the same original image analysis technique, in the present study we sought to evaluate the role of 4-dimensional (4D; 3-dimensional [3D]+ time) CT in the analysis of BAV and to describe the dynamics of the different morphotypes of BAV with regard to the latest expert consensus classification.[7]

METHODS

Ethics Statement

Ethics approval was waived by the Institutional Ethics Committee of Assistance Publique des Hôpitaux de Paris in a view of the study's retrospective nature and because all procedures were part of routine care (CERAPHP.5 00011928; February 19, 2019). All subjects were informed in writing that unless they objected, all data in their medical records, including cardiac images, could be used for research and scientific publications.

Population

Over a 6-month period, from the imaging database of 2 French institutions (Hôpital Européen Georges Pompidou and Limoges University Hospital), we included 15 consecutive patients with BAV who had undergone ECG-gated CT and echocardiography within 6 weeks. Subjects were age >18 years and in sinus rhythm with no significant coronary artery stenosis (>50%). Exclusion criteria were greater than moderate aortic stenosis or regurgitation, ascending aortic diameter >45 mm, infective endocarditis, and previous cardiac surgery. BAV were further divided into subgroups according to the latest expert consensus classification as well as their CO.

We also analyzed CT scans of 15 patients with the same inclusion/exclusion criteria and who had a normal functioning TAV to compare aortic morphometrics in the study groups.

ECG-Gated CT Protocol and Image Reconstruction

The imaging protocol and reconstruction technique have been described previously.[10] In brief, retrospective ECG-gated acquisition of multiphase cardiac computed tomography (MCCT) were performed from the level of the carina to the apex of the heart in a craniocaudal direction. Images were reconstructed at 10% to 100% of the R-R interval in 10% increments. End-systole was identified as the phase of aortic valve closing; end-diastole (ED), as the phase of mitral valve closing.

Using an in-house software (Lattido) developed at Favaloro University (Buenos Aires, Argentina), annular delineation for all 10 temporal phases was performed with 9 orthogonal planes generated automatically every 20° around an approximated long axis of the left ventricular outflow tract (LVOT). Observers identified the 2 edges of the aortic annulus (AA) on each of these 9 planes to obtain 18 points, from which a 3D curve was generated using a cubic spline. A best-fit plane was adjusted to the spline and 3 additional planes were created automatically for manual inner contouring of the other aortic root components. Two planes were generated 10 mm distant to the best-fit AA plane at the level of the LVOT and the level of sinus of Valsalva. The third plane, defined as the sinotubular junction, intercepted the 3 higher points of the AA. This procedure was repeated for all 10 temporal phases of the cardiac cycle.

The software allows calculation of geometric features, including 3D and projected 2D parameters. To calculate the AA area in 3D, triangles were formed between 2 consecutive points on the spline in 3D, delineating the border of the annulus and the AA centroid of the 18 seed points. The AA area was then calculated as the sum of each triangle's area. The perimeter was estimated as the length of the interpolated spline in 3D. For 2D measurements, a best-fit plane was adjusted to the 18 seed points of each time phase using a principal component analysis approach. AA area was estimated in 2D, projecting the spline points into the best-fit plane. The height of the annulus was estimated as the sum of distances of the farthest points on the 3D spline describing the AA below and above the best-fit plane. The longest distance between each pair of opposite points around the TA was

adopted as the maximal diameter value, and the distance between the pair of points orthogonal to the maximal diameter was called orthogonal to maximal diameter. The eccentricity index was calculated using the following formula:

$$Eccentricity = \sqrt{1 - \left(\frac{Orthogonal\ to\ maximal\ diameter}{Maximal\ diameter}\right)^2}$$

Statistical Analysis

Analyses were done using SPSS 26.0 (IBM). Continuous variables were reported as mean ± SD, and their normality of distribution was tested using the Shapiro-Wilk test. Comparisons between 3D and 2D areas, perimeters, and diameters were performed using the 2-tailed *t* test. Comparisons for categorical data were performed using the χ^2 test. Statistical significance between parameters was defined as $P < .05$.

RESULTS

Table 1 presents the general characteristics of the study population. The mean patient age was 54 ± 13 years in the BAV group and 58 ± 11 years in the TAV group ($P = .74$). Eighty percent of the BAV phenotypes were Sievers type I with a predominant left/right commissural fusion.

AA 3D Representation

Figure 1 shows the 3D curve of the AA generated using a cubic spline after pinpointing the 18 points on the annulus border. The 3D curve analysis allowed us to distinguish the 3 types of BAV: the 2-sinus type (Figure 1, *A*), fused type (Figure 1, *B*), and partial-fusion type (form fruste; Figure 1, *C*). The position and the height of the nonfunctional ("fused") commissure as well as the CO can be readily assessed.

Dimensions of the Aortic Root

We classified BAVs into 2 subgroups according to their CO: symmetrical BAV (CO 160°-180°) and asymmetrical BAV (CO 120°-140°). In our study population, we did not have subjects with a CO of 140°-160°. In total, 7 subjects had a symmetrical BAV, and 8 subjects had an asymmetrical BAV.

Table 2 shows the mean AA morphometrics in both groups. The BAV annulus was significantly larger than TAV annulus in terms of 3D/2D areas, perimeter, diameter, and height ($P < .001$). There were no differences between the 2 subtypes of BAV.

The sinuses of Valsalva and the sinotubular junction also were significantly larger in the BAV group compared to the TAV group (Table 3). There was no difference in the LVOT-indexed area between the 2 groups. All these findings remained constant throughout the cardiac cycle.

Analysis of BAV Subtypes and Comparison to TAV

Table 4 shows the relative height of the nonfunctional commissure relative to the least square plane of the annulus compared to the normal commissures. In symmetrical BAV, the nonfunctional commissure was significantly lower than the other 2 functional commissures ($P < .001$), whereas in asymmetrical BAV, the 3 commissures were of comparable height ($P = .32$).

Table 5 shows the eccentricity index (EI) of the different components of the aortic root at ED. Although there were no differences in the EI of the AA, the LVOT was more elliptical in TAV compared to asymmetrical BAV ($P = .023$) or symmetrical BAV ($P = .008$). On the other hand, sinuses of Valsalva were more circular in TAV and asymmetrical BAV compared to symmetrical BAV ($P = .002$).

Figure 2 shows the differences in EI for the aortic root. At ED, going from TAV to asymmetrical BAV to symmetrical

TABLE 1. Demographic data

Characteristic	BAV (N = 15)	TAV (N = 15)	*P* value
Age, y, mean ± SD	55 ± 13	58 ± 11	.74
Male sex, n (%)	15 (100)	5 (33.3)	<.001
Body surface area, mean ± SD	1.95 ± 0.16	1.75 ± 0.3	.03
Ejection fraction, %, mean ± SD	60.6 ± 1.8	59.2 ± 7.8	.87
Indication for CT scan, n (%)			
BAV evaluation	11 (73.3)	0 (0)	
Chest pain	3 (20.0)	8 (53.3)	
Arrythmias	0 (0)	5 (33.3)	
Other	1 (6.7)	2 (13.4)	
Sievers classification, n (%)			
Type 0	3 (20.0)		
Type 1	12 (80.0)		
L/R	8		
N/R	3		
N/L	1		

BAV, Bicuspid aortic valve; *TAV*, tricuspid aortic valve; *CT*, computed tomography; *L*, left; *R*, right; *N*, noncoronary.

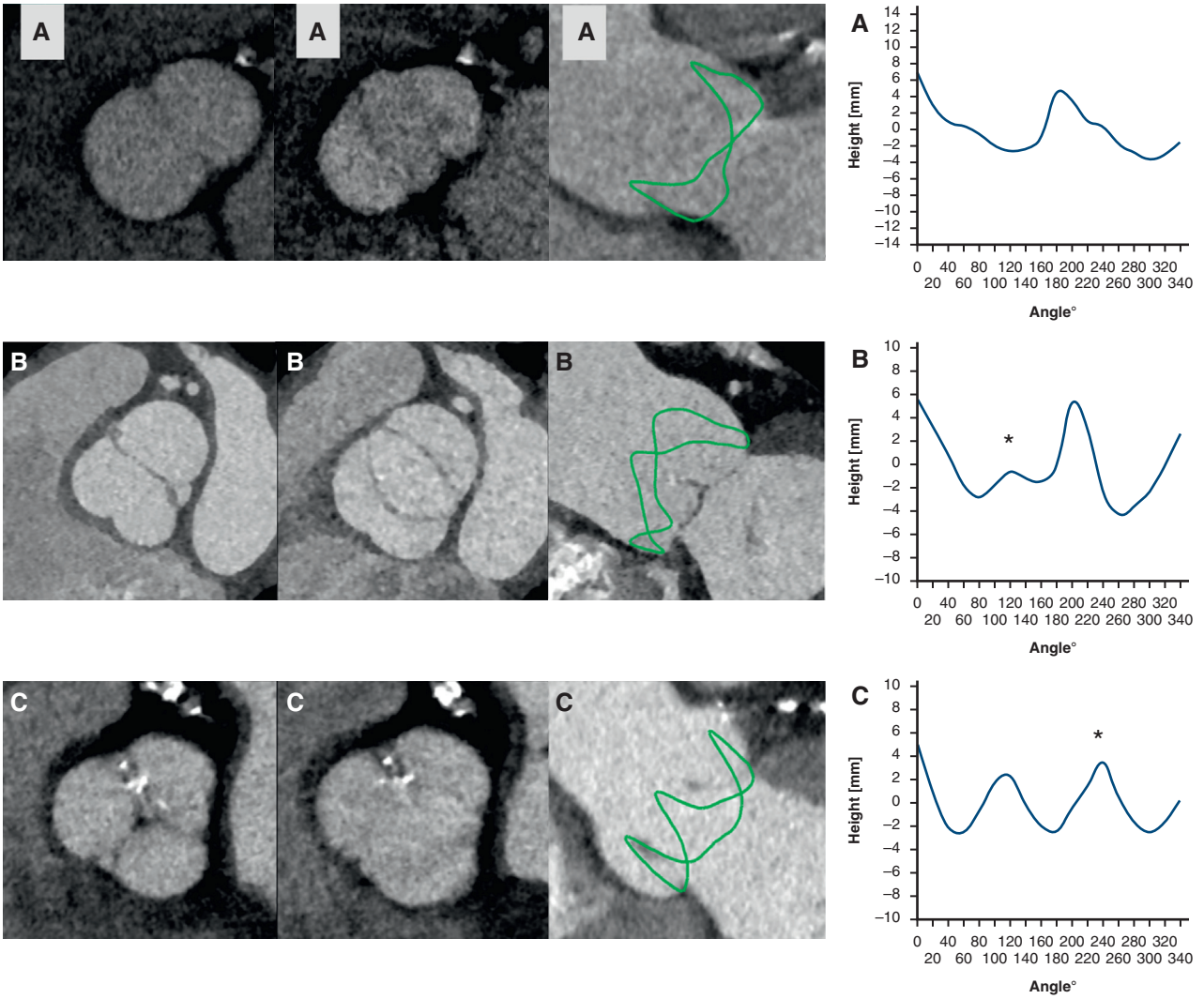

FIGURE 1. Aortic annulus (*AA*) automated contouring representation using our in-house software: aspect of the valve in diastole and systole, 3-dimensional representation of the AA (*green curve*), and projection (mean, 10 phase aspect) for each subtype of bicuspid aortic valve. A, 2-sinus type; B, fused type; C, partial-fusion type. *Nonfunctional commissure.

TABLE 2. CT measurements of the aortic annulus

Measurement	TAV (N = 15), mean ± SD	BAV (N = 15), mean ± SD	*P* value	Symmetrical (N = 7), mean ± SD	Asymmetrical (N = 8), mean ± SD	*P* value
Mean 3D area, cm^2	7.58 ± 1.59	10.97 ± 1.52	<.001	10.47 ± 1.29	11.41 ± 1.65	.24
Mean indexed 3D area, cm^2/m^2	4.3 ± 0.38	5.64 ± 0.84	<.001	5.20 ± 0.7	6.02 ± 0.79	.06
Mean 2D area, cm^2	5.14 ± 1.24	7.58 ± 0.99	<.001	7.45 ± 0.77	7.68 ± 1.19	.67
Mean 2D indexed area, cm^2/m^2	2.91 ± 0.34	3.89 ± 0.54	<.001	3.69 ± 0.32	4.06 ± 0.65	.19
Mean 3D perimeter, cm^2	11.75 ± 1.29	13.88 ± 1.22	<.001	13.45 ± 1.56	14.27 ± 1.21	.2
Mean 2D diameter, cm	2.5 ± 0.31	3.07 ± 0.26	<.001	3.05 ± 0.43	3.09 ± 0.43	.84
Height, mm	16.7 ± 2.2	21.81 ± 3.82	<.001			

CT, Computed tomography; *TAV*, tricuspid aortic valve; *BAV*, bicuspid aortic valve; *3D*, 3-dimensional; *2D*, 2-dimensional.

TABLE 3. CT-indexed areas of the aortic root components

Component	BAV (N = 15), cm^2/m^2	TAV (N = 15), cm^2/m^2	*P* value
LVOT			
ED	3.72 ± 0.41	3.45 ± 0.99	.41
ES	3.04 ± 0.55	2.81 ± 0.87	.45
Valsalva			
ED	6.06 ± 1.00	4.69 ± 1.00	<.001
ES	5.83 ± 0.94	4.67 ± 1.08	.004
STJ			
ED	5.13 ± 1.62	3.62 ± 0.99	.001
ES	5.25 ± 1.63	3.64 ± 1.17	.001

CT, Computed tomography; *BAV*, bicuspid aortic valve; *TAV*, tricuspid aortic valve; *LVOT*, left ventricular outflow tract; *ED*, end-diastole; *ES*, end-systole; *STJ*, sinotubular junction.

BAV, the LVOT became more circular and the sinuses of Valsalva became more elliptical, whereas EI of the AA remained the same.

DISCUSSION

BAV, a common congenital heart disease, is a complex entity characterized by heterogeneous morphologic features and pathologies. Comprehensive evaluation of the morphologic aspects of BAV is mandatory, especially in the era of TAVR and root repair surgeries. In this study, we used an innovative image analysis method for BAV based on 4D MCCT and specific software developments. Our technique enables a 3D dynamic evaluation of the AA throughout the cardiac cycle with easy assessment of BAV morphology, nonfunctional commissural features, and commissural orientation. BAV represents a spectrum of morphology with significant differences in the aspect of the aortic root between the different types of BAV.

CT Evaluation of BAV Morphology

CT is the imaging modality of choice in the preoperative evaluation of BAV. Whereas standard valve analysis consists of scrolling through transverse images or performing double-oblique multiplanar reconstructions, some authors have proposed novel analysis techniques. Amoretti and colleagues[11] proposed a multiplanar analysis based on complete visualization of the line of insertion of the valve leaflets and the interleaflet triangles. Categorization of BAV anatomy then would be based on the degree of underdevelopment (or on the absence) of 1 interleaflet triangle. Devos and colleagues[12] proposed the use of a new sign, the "hammock" sign, on standard coronal images, inspired by the occasional depiction of a BAV spanning the entire width of the aortic sinus on a coronal or sagittal reconstruction, with its curve resembling a hammock. Our analysis technique does not necessarily distinguish all forms of BAV, since the 3D representation of the AA of a very asymmetrical BAV is similar to that of TAV. However, our method provides more detailed information on the BAV morphology, especially with regard to the height and the position of the nonfunctional commissure as well as the CO.

Along with the differences observed for the AA, the entire aortic root presents a spectrum of variability in its morphology within the different subtypes of BAV and compared to TAV. Actually, going from TAV to asymmetrical BAV to symmetrical BAV, the LVOT became more circular, and the sinuses of Valsalva became more elliptical. The EI of the AA remained the same. In their study, Chirichilli and colleagues[13,14] found a spectrum of AA ellipticity, with the AA being more elliptical in TAV and asymmetrical BAV and more circular in symmetrical BAV. However, in this study, the AA reflected the virtual basal ring and not the true 3D AA. Therefore, their results on the EI of the virtual basal ring are in accordance with our findings on the EI of the LVOT.

BAV in TAVR

For several years, BAV have been excluded from large randomized trials in TAVR because of their association with higher rates of paravalvular leak, new permanent pacemaker, and annular rupture compared to TAV.[15] Several factors make TAVR more challenging in BAV compared to TAV: BAV often is more calcified, the aortic root is more elliptical, and the AA is typically larger.[16] Several recent observational studies have suggested improved outcomes for TAVR in BAV, driven by improvements in device technology, implantation techniques, and imaging screening.[17,18]

TABLE 4. Commissure height by subtype of BAV

Subtype	Commissure 1, mm, mean ± SD	Commissure 2, mm, mean ± SD	Nonfunctional commissure, mm, mean ± SD	*P* value
Symmetrical (n = 7)	18.24 ± 3.20	17.15 ± 3.60	6.01 ± 4.27	<.001
Asymmetrical (n = 8)	16.38 ± 0.86	15.88 ± 1.69	15.37 ± 0.88	.32

BAV, Bicuspid aortic valve.

TABLE 5. EI of the aortic root components in TAV and subgroups of BAV at end-diastole

Component	TAV (N = 15)	Symmetrical BAV (N = 7)		Asymmetrical BAV (N = 8)	
	EI	EI	*P* value	EI	*P* value
LVOT	0.74	0.61	.023	0.6	.008
AA	0.49	0.49	.06	0.52	.30
Valsalva	0.28	0.19	.070	0.47	.002

EI, Eccentricity index; *TAV*, tricuspid aortic valve; *BAV*, bicuspid aortic valve; *LVOT*, left ventricular outflow tract; *AA*, aortic annulus.

In this regard, standard sizing for BAV has not yet been developed. Prosthesis sizing based on a virtual basal ring evaluation is the gold standard in TAV stenosis. Most previous studies used prosthesis sizing based on virtual basal ring area measurement in BAV.[19,20] Others opted for a supra-annular sizing at the level of maximal constraint[21] or with the LIRA (level of implantation at the raphe) technique.[22] However, we have previously demonstrated that VBR

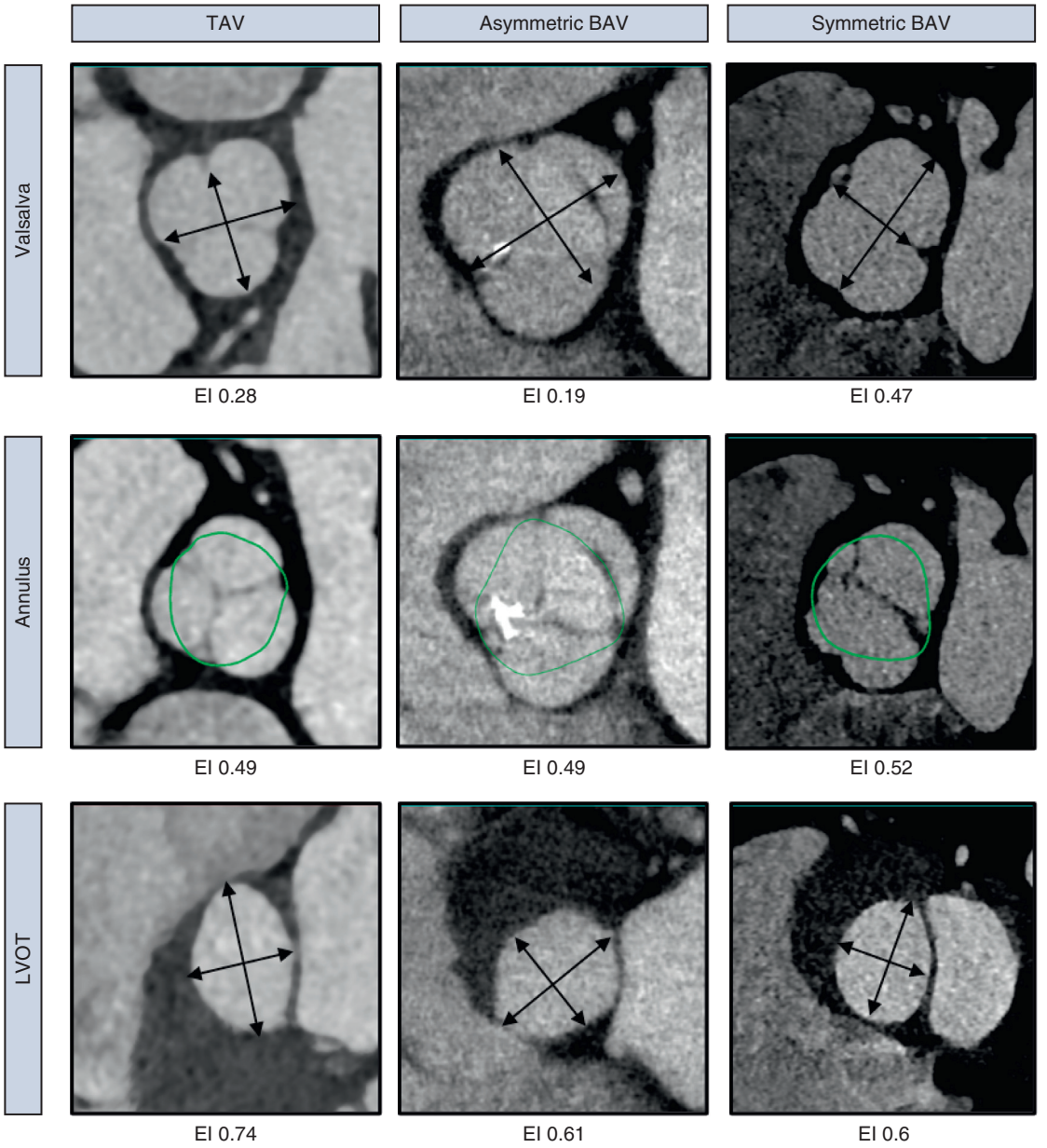

FIGURE 2. Summary of the eccentricity indexes in end-diastole of the aortic root in tricuspid aortic valves (*TAVs*) and bicuspid aortic valves (*BAVs*). *EI*, Eccentricity index; *LVOT*, left ventricular outflow tract.

analysis significantly underestimated the 3D and projected 2D dimensions of the true AA in normal functioning TAV.[10] Moreover, Ciobotaru and colleagues[23] found that the use of 3D analysis might reduce the risk of paravalvular regurgitation following TAVR in TAV patients. Whether annular sizing (2D projected area and perimeter) using our 4D method that includes a 3D temporal analysis technique provides a solution to prosthesis sizing in TAVR for BAV stenosis is yet to be demonstrated through dedicated studies, but our results suggest that the varied morphology of AA in the different BAV types should be considered for optimal prosthesis sizing. Furthermore, whether the spectrum of ellipticity between the different subtypes of BAV persists in heavily calcified stenotic BAV remains to be demonstrated.

BAV in Aortic Root Surgeries

Improved techniques in aortic root surgery have been associated with improved durability of the aortic repair.[24] Several challenges remain in the BAV repair, owing essentially to BAV polymorphism. Additionally, several anatomic characteristics have been reported as predictors of valve repair failure, including partial fusion and very asymmetrical CO.[25,26]

Owing to the heterogeneity in BAV morphology, De Kerchove and colleagues[8] proposed a new repair-based classification based on the CO. Patients with symmetrical CO (160°-180°) were treated with central plication without modification of the commissural angle. Patients with asymmetrical commissural orientation (140°-160°) were treated by increasing the commissural angle to 180°. Patients with very asymmetrical commissural orientation (120°-140°) were treated like those with a trileaflet valve. In this context, preoperative CT assessment of the aortic valve is of utmost importance to evaluate AA morphology in BAV. Our analysis technique provides an excellent overview of the AA morphology (commissural orientation in particular) and also allows visualization of the position and height of the nonfunctional commissure, guiding annuloplasty.

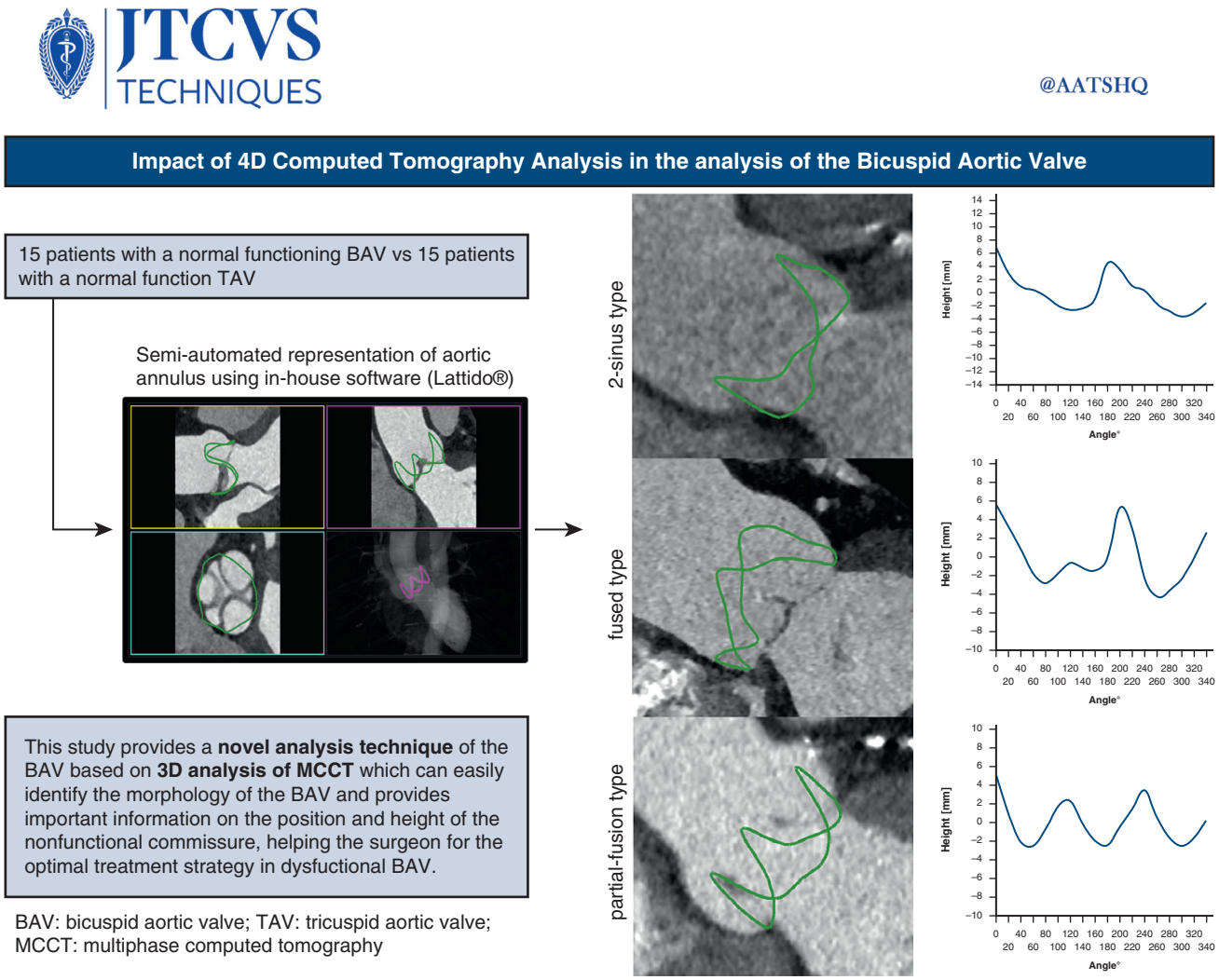

FIGURE 3. Graphical abstract.

Limitations

This study is a retrospective bicenter study with a small sample size, and our results should be validated in larger populations. Although we indexed the measurements of the aortic root to body surface area, the differences in sex distribution and thus body surface area in BAV and in TAV might impact our results. Our results reflect the morphology of normal BAV. Further studies are needed to evaluate pathologic BAV (stenosis or regurgitation) and to analyze the impact of 4D analysis in clinical practice.

CONCLUSIONS

This study confirms the significant morphologic differences of the aortic root between TAV and BAV in terms of its dimensions and between the different morphotypes of BAV, mainly in the EI (Figure 3). This study also describes a novel BAV analysis technique based on 3D MCCT, which can readily identify the morphology of the BAV and provide important information on the position and height of the nonfunctional commissure that can contribute to determining the optimal treatment strategy for dysfunctional BAV.

Conflict of Interest Statement

The authors reported no conflicts of interest.

The *Journal* policy requires editors and reviewers to disclose conflicts of interest and to decline handling or reviewing manuscripts for which they may have a conflict of interest. The editors and reviewers of this article have no conflicts of interest.

References

1. Michelena HI, Prakash SK, Della Corte A, et al. Bicuspid aortic valve: identifying knowledge gaps and rising to the challenge from the International Bicuspid Aortic Valve Consortium (BAVCon). *Circulation*. 2014;129(25):2691-2704.
2. Della Corte A, Body SC, Booher AM, et al. Surgical treatment of bicuspid aortic valve disease: knowledge gaps and research perspectives. *J Thorac Cardiovasc Surg*. 2014;147(6):1749-1757.e1. https://doi.org/10.1016/j.jtcvs.2014.01.021
3. Habchi KM, Ashikhmina E, Vieira VM, et al. Association between bicuspid aortic valve morphotype and regional dilatation of the aortic root and trunk. *Int J Cardiovasc Imaging*. 2017;33(3):341-349. https://doi.org/10.1007/s10554-016-1016-8
4. Sievers HH, Schmidtke C. A classification system for the bicuspid aortic valve from 304 surgical specimens. *J Thorac Cardiovasc Surg*. 2007;133(5):1226-1233. https://doi.org/10.1016/j.jtcvs.2007.01.039
5. Schaefer BM, Lewin MB, Stout KK, et al. The bicuspid aortic valve: an integrated phenotypic classification of leaflet morphology and aortic root shape. *Heart*. 2008;94(12):1634-1638. https://doi.org/10.1136/hrt.2007.132092
6. Jilaihawi H, Chen M, Webb J, et al. A bicuspid aortic valve imaging classification for the TAVR era. *JACC Cardiovasc Imaging*. 2016;9(10):1145-1158. https://doi.org/10.1016/j.jcmg.2015.12.022
7. Michelena HI, Della Corte A, Evangelista A, et al. International consensus statement on nomenclature and classification of the congenital bicuspid aortic valve and its aortopathy, for clinical, surgical, interventional and research purposes. *Eur J Cardiothorac Surg*. 2021;60(3):448-476. https://doi.org/10.1093/ejcts/ezab038
8. de Kerchove L, Mastrobuoni S, Froede L, et al. Variability of repairable bicuspid aortic valve phenotypes: towards an anatomical and repair-oriented classification. *Eur J Cardiothorac Surg*. 2019;56(2):351-359. https://doi.org/10.1093/ejcts/ezz033
9. Tanaka R, Yoshioka K, Niinuma H, Ohsawa S, Okabayashi H, Ehara S. Diagnostic value of cardiac CT in the evaluation of bicuspid aortic stenosis: comparison with echocardiography and operative findings. *AJR Am J Roentgenol*. 2010;195(4):895-899. https://doi.org/10.2214/AJR.09.3164
10. Fikani A, Craiem D, Mousseaux E, et al. Morphological and dynamic analysis of the normal aortic valve with 4D computed tomography. *Eur J Cardiothorac Surg*. 2024;65(4):ezae113. https://doi.org/10.1093/ejcts/ezae113
11. Amoretti F, Cerillo AG, Mariani M, Stefano P. A simple method to visualize the bicuspid aortic valve pathology by cardiac computed tomography. *J Cardiovasc Comput Tomogr*. 2020;14(2):195-198. https://doi.org/10.1016/j.jcct.2019.08.005
12. Devos D, Van Langenhove C, Campens L. The hammock sign in computed tomography as a detection aid for bicuspid aortic valves. *J Belg Soc Radiol*. 2023;107(1):5. https://doi.org/10.5334/jbsr.2974
13. Chirichilli I, Irace FG, Weltert LP, et al. A direct correlation between commissural orientation and annular shape in bicuspid aortic valves: a new anatomical and computed tomography classification. *Interact Cardiovasc Thorac Surg*. 2020;30(5):666-670. https://doi.org/10.1093/icvts/ivz325
14. Chirichilli I, Irace F, Weltert L, et al. Morphological modification of the aortic annulus in tricuspid and bicuspid valves after aortic valve reimplantation: an electrocardiography-gated computed tomography study. *Eur J Cardiothorac Surg*. 2019;56(4):778-784. https://doi.org/10.1093/ejcts/ezz065
15. Yoon SH, Bleiziffer S, De Backer O, et al. Outcomes in transcatheter aortic valve replacement for bicuspid versus tricuspid aortic valve stenosis. *J Am Coll Cardiol*. 2017;69(21):2579-2589. https://doi.org/10.1016/j.jacc.2017.03.017
16. Philip F, Faza NN, Schoenhagen P, et al. Aortic annulus and root characteristics in severe aortic stenosis due to bicuspid aortic valve and tricuspid aortic valves: implications for transcatheter aortic valve therapies. *Catheter Cardiovasc Interv*. 2015;86(2):E88-E98. https://doi.org/10.1002/ccd.25948
17. Deeb GM, Reardon MJ, Ramlawi B, et al. Propensity-matched 1-year outcomes following transcatheter aortic valve replacement in low-risk bicuspid and tricuspid patients. *JACC Cardiovasc Interv*. 2022;15(5):511-522. https://doi.org/10.1016/j.jcin.2021.10.027
18. Forrest JK, Ramlawi B, Deeb GM, et al. Transcatheter aortic valve replacement in low-risk patients with bicuspid aortic valve stenosis. *JAMA Cardiol*. 2021;6(1):50-57. https://doi.org/10.1001/jamacardio.2020.4738
19. Sannino A, Cedars A, Stoler RC, Szerlip M, Mack MJ, Grayburn PA. Comparison of efficacy and safety of transcatheter aortic valve implantation in patients with bicuspid versus tricuspid aortic valves. *Am J Cardiol*. 2017;120(9):1601-1606. https://doi.org/10.1016/j.amjcard.2017.07.053
20. Tchetche D, de Biase C, van Gils L, et al. Bicuspid aortic valve anatomy and relationship with devices: the BAVARD multicenter registry. *Circ Cardiovasc Interv*. 2019;12(1):e007107. https://doi.org/10.1161/CIRCINTERVENTIONS.118.007107
21. Xiong TY, Feng Y, Li YJ, et al. Supra-annular sizing for transcatheter aortic valve replacement candidates with bicuspid aortic valve. *JACC Cardiovasc Interv*. 2018;11(17):1789-1790. https://doi.org/10.1016/j.jcin.2018.06.002
22. Iannopollo G, Romano V, Buzzatti N, et al. A novel supra-annular plane to predict TAVI prosthesis anchoring in raphe-type bicuspid aortic valve disease: the LIRA plane. *EuroIntervention*. 2020;16(3):259-261. https://doi.org/10.4244/EIJ-D-19-00951
23. Ciobotaru V, Maupas E, Dürrleman N, et al. Predictive value for paravalvular regurgitation of 3-dimensional anatomic aortic annulus shape assessed by multidetector computed tomography post-transcatheter aortic valve replacement. *Eur Heart J Cardiovasc Imaging*. 2016;17(1):85-95. https://doi.org/10.1093/ehjci/jev128
24. de Meester C, Vanovershelde JL, Jahanyar J, et al. Long-term durability of bicuspid aortic valve repair: a comparison of 2 annuloplasty techniques. *Eur J Cardiothorac Surg*. 2021;60(2):286-294. https://doi.org/10.1093/ejcts/ezaa471
25. Schneider U, Feldner SK, Hofmann C, et al. Two decades of experience with root remodeling and valve repair for bicuspid aortic valves. *J Thorac Cardiovasc Surg*. 2017;153(4):S65-S71. https://doi.org/10.1016/j.jtcvs.2016.12.030
26. Aicher D, Kunihara T, Abou Issa O, Brittner B, Gräber S, Schäfers HJ. Valve configuration determines long-term results after repair of the bicuspid aortic valve. *Circulation*. 2011;123(2):178-185. https://doi.org/10.1161/CIRCULATIONAHA.109.934679

Key Words: bicuspid aortic valve, aortic root, aortic annulus, computed tomography